J Nondestruct Eval
DOI 10.1007/s10921-014-0225-0

Dynamic Acousto-Elasticity in a Fatigue-Cracked Sample

J. Rivière · M. C. Remillieux · Y. Ohara · B. E. Anderson · S. Haupert · T. J. Ulrich · P. A. Johnson

Received: 14 November 2013 / Accepted: 15 January 2014

Abstract Dynamic acousto-elasticity (DAE) provides a unique way to observe nonlinear elastic features over an entire dynamic stress cycle including hysteresis and memory effects, detailing the full nonlinear behavior under tension and compression. This supplemental information cannot be observed with conventional nonlinear ultrasonic methods such as wave frequency mixing or resonance measurements, since they measure average, bulk variations of modulus and attenuation versus strain level. Where prior studies have employed DAE in volumetrically nonlinear materials (*e.g.*, rocks, bone with distributed micro-crack networks), here we report results of DAE on the application to a single localized nonlinear feature, a fatigue crack, to characterize the nonlinear elastic response in regions of the crack length, tip, and undamaged portions of an aluminum sample. Linear wave speed, linear attenuation and third order elastic moduli (i.e., nonlinear parameters) each indicate a sensitivity to the presence of the crack, though in unique manners. The localized nature of the DAE measurement and its potential for quantifying all of the third order elastic constants makes it a promising technique for both detecting cracks, as well as providing quantitative information on the effect of the cracks on the material integrity.

J. Rivière (✉) · M. C. Remillieux · B. E. Anderson · T. J. Ulrich · P. A. Johnson
Geophysics Group MS D446, Earth and Environmental Sciences, Los Alamos National Laboratory, Los Alamos, NM 87545, USA
e-mail: riviere_jacques@yahoo.fr

Y. Ohara
Department of Materials Processing, Graduate School of Engineering, Tohoku University, 02 Aoba Aramaki, Sendai 980-8579, Japan

S. Haupert
Laboratoire d'Imagerie Parametrique, University of Paris VI, UPMC, CNRS, Paris, France

Keywords Nondestructive evaluation · Nonlinear ultrasound · Nonlinear acoustics · Dynamic acousto-elasticity · Fatigue crack

1 Introduction

Probing elastic nonlinearity of materials has broad application including medical imaging, engineering and geophysics, as elastic nonlinearity is a sensitive measure of mechanical damage in solids at many length scales. The dynamic acousto-elastic (DAE) technique probes the nonlinear elastic response in a localized region and then provides a complimentary method for local inspection of material integrity when compared to bulk nonlinear techniques.

In standard (*i.e.*, static) acousto-elasticity, ultrasonic or acoustic waves propagate through the specimen while it is statically stressed at different magnitudes (uniaxial or hydrostatic stress) [1,2]. For isotropic materials, the change in speed of sound with stress levels allows one to extract the third order elastic constants A, B, C [3]. For practical reasons, the applied stress is usually only compressive and static strain levels must be relatively high to be measured properly ($>10^{-4}$).

DAE employs a low frequency wave source instead of a static device to stress the rod shaped sample at its fundamental compressional mode. Strain levels are therefore smaller (10^{-8} to 10^{-5}), and the sample is tested under both compression and tension allowing one to obtain the elastic response over a complete dynamic stress cycle. Previous DAE results [4–6] have shown complex elastic nonlinearity signatures, in particular hysteretic behaviors and strong effects of material *conditioning* [7–9].

DAE falls under the broad category of *pump-probe* methods that have existed in nonlinear acoustics from at least the

Published online: 28 January 2014

1950s [10–13]. It involves application of two dynamic fields, one to perturb the material elasticity (the *pump*) and one to measure the induced elastic changes (the *probe*). DAE uses a low frequency *pump* (LF field) and a high frequency pulses as a *probe* (HF field).

Our intent is to explore DAE techniques to characterize localized damage in metal. An aluminum sample containing a single closed crack due to fatigue cycling is investigated. Linear and nonlinear parameters are compared with respect to the crack features.

2 Materials and Methods

2.1 Sample

A closed fatigue crack was formed in an aluminum alloy specimen (A7075) by a three-point bending fatigue test. Dimensions of the sample are $L = 170$ mm, $L_y = 30$ mm, $L_z = 40$ mm. The fatigue crack was extended from a notch placed at mid-length ($x = h = L/2$) with a maximum stress intensity factor $K_{max} = 4.3MPa * m^{1/2}$ and a minimum stress intensity factor $K_{min} = 0.6MPa * m^{1/2}$ [14,15]. The fatigue crack is in the plane normal to the x-axis, invisible to the eye. The notch is approximately 3mm deep, the fatigue crack is 17 mm long on the sample sides and a few millimeters longer at the sample center, as the central and edge parts are under plane strain and plane stress conditions, respectively [16,17]. The crack, therefore, penetrates to a depth of approximately half the sample width ($L_z/2 = 3 + 17$ mm).

2.2 Experimental System

2.2.1 DAE setup

The sample shown in Fig. 1a stands upright on a low frequency compressional source, a piezoceramic disk. A high frequency compressional source and associated receiver (Olympus V323-N-SU, Japan) straddle the sample on each side of the crack, propagating a longitudinal wave along the y-axis. The essential idea is to have a high frequency broadcast, from ultrasonic source to ultrasonic receiver, to probe the elastic state that is modulated in the sample by the low frequency source. Ultrasonic gel is used to ensure good coupling between the sample and the transducers. We also put a thin layer of adhesive tape on the sample to prevent the gel from entering the crack. The low frequency f_{LF} is the frequency of the lowest compressional resonant mode of the cylinder, $f_{LF} = c/(4L)$ with fixed-free boundary conditions (wavelength $\lambda_{LF} = 4L$) and where c is the nominal compressional sound speed in the sample [9].

The strain field is sampled at $x = h$ by the high frequency broadcast that crosses the sample in time, t_{US}, of order

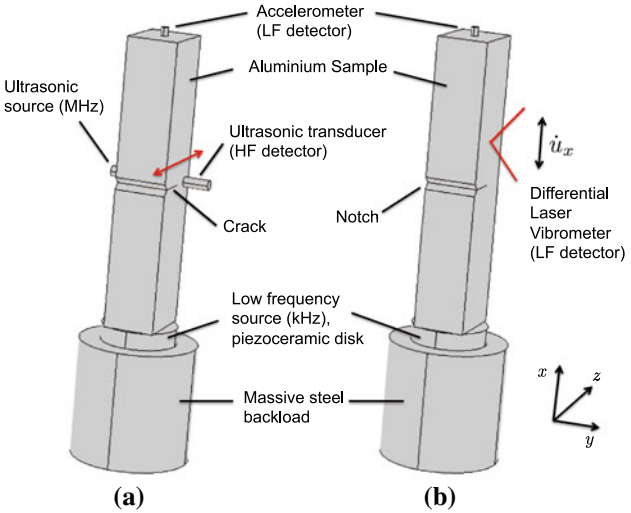

Fig. 1 **a** DAE setup. The low frequency source resonates the sample at its first compressional mode (≃7000 Hz), with approximately fixed-free boundary conditions [9]. Ultrasound pulses at 2 MHz are launched in the sample simultaneously to probe the sample at a given strain level imposed by the low frequency field. An accelerometer is placed on the top of the sample to measure the low frequency field whereas a second ultrasonic transducer detects the high frequency pulses. The two ultrasonic transducers are placed on opposite sides of the crack so that the longitudinal ultrasonic wave propagates along the crack. The *double red arrow* indicates that the two transducers can be translated along the sample width to probe the crack at different locations (from the notch to the tip). **b** LF strain field setup. A differential laser vibrometer is used to map the axial strain ϵ_x along the sample side, deduced from the measured particle velocity $\dot{u}_x$ (Color figure online)

$d/c \simeq 10\mu s$. During the high frequency wave travel time the low frequency strain field changes very little, $t_{US}/T_{LF} = d/(4L) = 3/68 \simeq 0.05$, with $T_{LF} = 1/f_{LF}$. This first condition is required to assume an acousto-elastic effect ($t_{US} << T_{LF}$). Further, the ultrasonic (US) signal recorded at the US receiver propagates mostly within a diameter beam corresponding to the diameter of the US transducer ($d_{US} = 6$ mm). Thus we can assume that the strain established in the sample by the low frequency source is constant spatially over the US beam width ($d_{US}/\lambda_{LF} = 0.6/68 \simeq 0.01$) [4–6].

Assuming fixed-free boundary conditions and a beam sample with no notch and no crack, the strain ϵ_x is maximum at $x = 0$ and can be evaluated from the acceleration $\ddot{u}_x$ measured at the top of the sample using $\epsilon_x(0,t) = -\ddot{u}_x(L,t)/(8\pi L f_{LF}^2)$. The strain at $x = h$ is then found using $\epsilon_x(h,t) = \epsilon_x(0,t)\cos\left(\frac{\pi h}{2L}\right) = \epsilon_x(0,t)/\sqrt{2}$ [18]. This strain evaluation assumes a regular beam with no notch and no crack as a first approximation. The second experiment described in the next section (Sect. 2.2.3) will then be used to refine our results, using experimental evaluation of the strain field in the material.

The high frequency source at 2MHz is a pulse of duration 1.5 μs *i.e.*, three high frequency periods. The spacing time ΔT between two consecutive pulses is chosen such that

the coda signal received in response to the jth pulse decays to zero before sending the $(j+1)$th pulse. Further, ΔT is chosen to be incommensurate with T_{LF}, so that over time the broadcasts at the set of times $\{t_j\}$ sample all phases of the LF strain field. For this aluminium sample, we choose $\Delta T = 2$ ms. The low frequency broadcast/detection and the high frequency broadcast/detection are controlled by a central clock. Both detections are sampled at 50 MHz.

Each pulse propagating during the steady-state is compared with the pulses that traverse the sample before activation of the low frequency source by employing cross-correlation. This allows the determination of $\tau(t_j)$, the shift in the time of flight of the high frequency pulse as it crosses the sample at time t_j [19,20]. Time of flight modulations can be converted into a relative velocity change using:

$$\frac{\Delta c}{c}\left(t_j\right) = -\frac{\tau(t_j)}{t_{US}^0} \tag{1}$$

where t_{US}^0 is the time of flight of the reference pulse. Changes in the relative sound speed are associated with the strain field $\epsilon_x(h, t_j)$, at the moment of the high frequency broadcast, *i.e.*, $\frac{\Delta c}{c}(t_j) \Leftrightarrow \epsilon_x(h, t_j)$.

The DAE measurement is performed at 12 different locations by moving the two ultrasonic transducers along the sample width, ($x = h$, red arrow in Fig. 1a), starting from the notch side of the crack ($z = 4$ mm) up to $z = 37$ mm with a step $\Delta z = 3$ mm. Because the US transducers are 6 mm in diameter and we perform a measurement every 3 mm, there is a 50 % overlap between two adjacent measurements. Measurements are repeated three times with repositioning of the ultrasonic transducers and the gel. Error bars correspond to one standard deviation.

2.2.2 Linear Ultrasonic Measurements

To compare DAE (nonlinear) measurements with linear parameters, we also measure the linear ultrasonic velocity and attenuation at each location along the sample width, *i.e.* without applying the LF resonance. The velocity is extracted by estimating the time difference between the first arrival pulse (one way in the sample, L_y) and the second arrival pulse (three traverses of the sample, $3L_y$). The time difference is estimated precisely by calculating the autocorrelations of the signals. The attenuation is extracted by comparing the spectral amplitudes A_1 and A_2 of these two pulses:

$$\alpha = -\frac{\ln\left(\frac{3L_y}{L_y}\frac{A_2}{A_1}\right)}{2L_y} \tag{2}$$

where the ratio $\frac{3L_y}{L_y} = 3$ accounts for the fact that the propagation is not planar in the sample, but spherical [21], as observed in simulation results (Fig. 3). These measurements are performed at 12 different locations along the crack ($x = h$ and z varying from 4 to 37 cm). Some measurements are also performed far from the crack for comparison ($x = h+4$ cm). Linear measurements are also repeated three times with repositioning of the ultrasonic transducers and the gel, with error bars corresponding to one standard deviation.

2.2.3 LF Strain Scanning Setup

As described in Fig. 1b, a fiber-optic differential laser vibrometer [22,9] (Polytec OFV 552) can also be deployed to measure the axial vector velocity field ($\dot{u}_x$) of the sample side during activation of the LF source at the frequency of the first compressional mode. The spatial structure of the LF strain field and the influence of the notch and the crack can be then evaluated from this measurement. A first scan is performed on the full side of the sample, with $\Delta x = \Delta z = 6$ mm—resolution in both x and z directions. The displacement u_x is deduced from the particle velocity $\dot{u}_x$ with $u_x = \dot{u}_x/(2\pi f_{LF})$. The strain ϵ_x is then deduced from the displacement by computing the spatial derivative of the displacement, *i.e.*, $\epsilon_{x+\Delta x/2} = (u_{x+\Delta x} - u_x)/\Delta x$. A finer scan is also performed in the vicinity of the notch (0.1mm-resolution) to observe in more detail the strain field along the notch/crack.

2.3 Simulations: Propagation of the HF Probe

To better understand how ultrasonic pulses propagate along the crack, we simulate the linear analysis reported in Sect. 2.2.2, in the time domain, with a 2D undamped model of the ultrasonic wave propagation through the aluminum sample without and with cracks. The "Solid Mechanics" module of the commercial finite-element software package Comsol Multiphysics 4.3a was used for this purpose. The aluminum subdomain has a width of 30 mm and a height of 170 mm. We assume that the aluminum sample has a mass density of 2,700 kg/m^3, a Poisson's ratio of 0.33, and a Young's modulus of 70 GPa. The perturbation caused by the ultrasonic source is modeled as a horizontal displacement imposed on the boundary of the subdomain, over a length of 6 mm (diameter of the transducer) around the mid-height ($x = h$) of the sample. The time dependence of this displacement is that of a Ricker wavelet centered at 2 MHz with a peak amplitude of 1 µm. This wavelet is a zero-phase wavelet commonly used in seismology and acoustics to model impulsive excitations. It is identical to the second derivative of the Gaussian probability distribution function. The energy content of this wavelet decays rapidly beyond the center frequency, thus containing the numerical solution in a frequency range adapted to the spatial and temporal discretization of the problem [23]. The LF source and backload are not modeled. Instead, the bottom face of the aluminum sample is modeled with a fixed bound-

ary condition. The crack is modeled as a void cavity, with a uniform thickness of 1 μm throughout and a length equal to the full width of the sample. We assume that the crack has a perfectly rectangular geometry (flat crack). Transient responses were simulated from 0 to 20 μs, in steps of 10 ns.

The velocities and attenuations are extracted in the same way as for experiments (Sect. 2.2.2). The displacement at the receiver is averaged over its size (6 mm) to extract both parameters. The only small difference is in the calculation of the attenuation because of the 2D-simulation. Therefore, the correction coefficient in Eq. (2) becomes $\frac{\sqrt{3L_y}}{\sqrt{L_y}} = \sqrt{3}$, instead of 3 [21].

Changes in velocity and attenuation along the sample width can be compared with high frequency simulations described in Sect. 2.3 and presented in Fig. 3. In Fig. 2a, the velocity extracted from simulations remains unchanged whether the crack is present or not, and is slightly lower than that found experimentally.

In Fig. 2b, we find that attenuation found in simulation is similar to experimental results, although slightly lower. Figure 3 shows that the wave propagating along the crack partly deviates from its original path through the mechanism of mode conversion along the crack surface. This accounts for most of the difference between cracked and non cracked regions in Fig. 2b.

3 Results

3.1 HF Linear Velocity and Attenuation

In Fig. 2, we present the linear ultrasonic results (velocity and attenuation) obtained experimentally along the sample width. These results are obtained using only the two ultrasonic transducers, *i.e.*, without applying the low frequency resonance. The velocity is found to be slightly lower when the wave propagates along the crack. Far from the crack and near the sample boundaries (red stars in Fig. 2), the velocity is slightly higher (by approximately 30 m/s).The attenuation is found larger when the wave propagates along the crack, in contrast to non-cracked locations, where it is almost negligible.

3.2 LF Displacement and Strain Field

To evaluate the influence of the notch and the crack on the strain field in the sample, we undertake an investigation of the mode shape at the frequency of the first compressional mode (setup in Fig. 1b). Results of this measurement are displayed in Fig. 4.

One can observe the expected $\lambda/4$-profile for the displacement and strain of a fixed-free beam in Fig. 4a, b. However, we see a strain concentration near the notch/crack region [24]. In Fig. 4c, d, one can observe the strain concentration in more detail, starting from the notch $z = 3$ mm and extending up to $z \simeq 7$ mm. We did not observe any other strain concentration near the crack tip (not shown), suggesting that the crack is essentially closed from $z \simeq 7$ mm to its tip. Strain fields

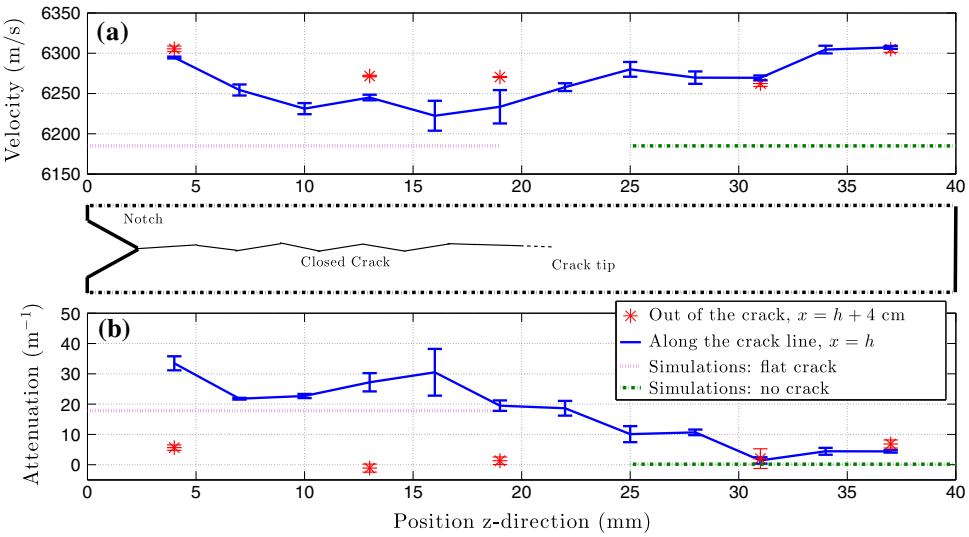

Fig. 2 Ultrasonic propagation: linear velocity and attenuation measurements. **a** Velocity as a function of the position along the crack ($x = h$). *Red stars* represent velocities measured far from the crack, along the width corresponding to $x = h + 4$ cm, for comparison. Simulation results are also presented for comparison (no crack and flat crack cases). **b** Attenuation as a function of the position along the crack. The crack tip is located approximately at $z = 20$ mm on the edges of the sample and few millimeters more in the center. A *dashed line* is sketched between $z = 20$ *and* 22 mm for this reason. Simulation results are also presented for comparison (no crack and flat crack cases) (Color figure online)

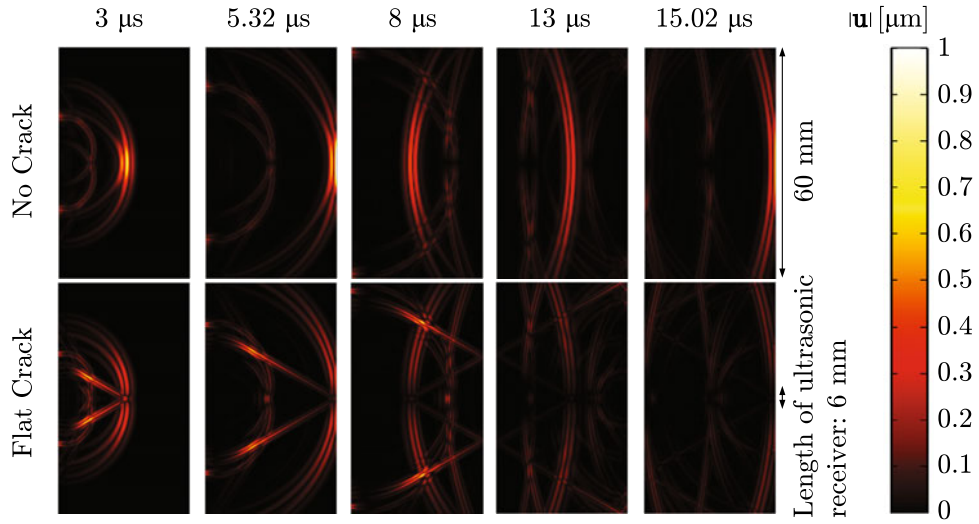

Fig. 3 Ultrasonic linear propagation: simulations. Snapshots at times 3, 5.32, 8, 13 and 15.02 µs are presented for two different cases: no crack and 1 µm-thick flat crack. Duration 5.32 µs corresponds to a one way transmission within the sample thickness L_y, while duration 15.02 µs corresponds to one round trip and a half within the sample

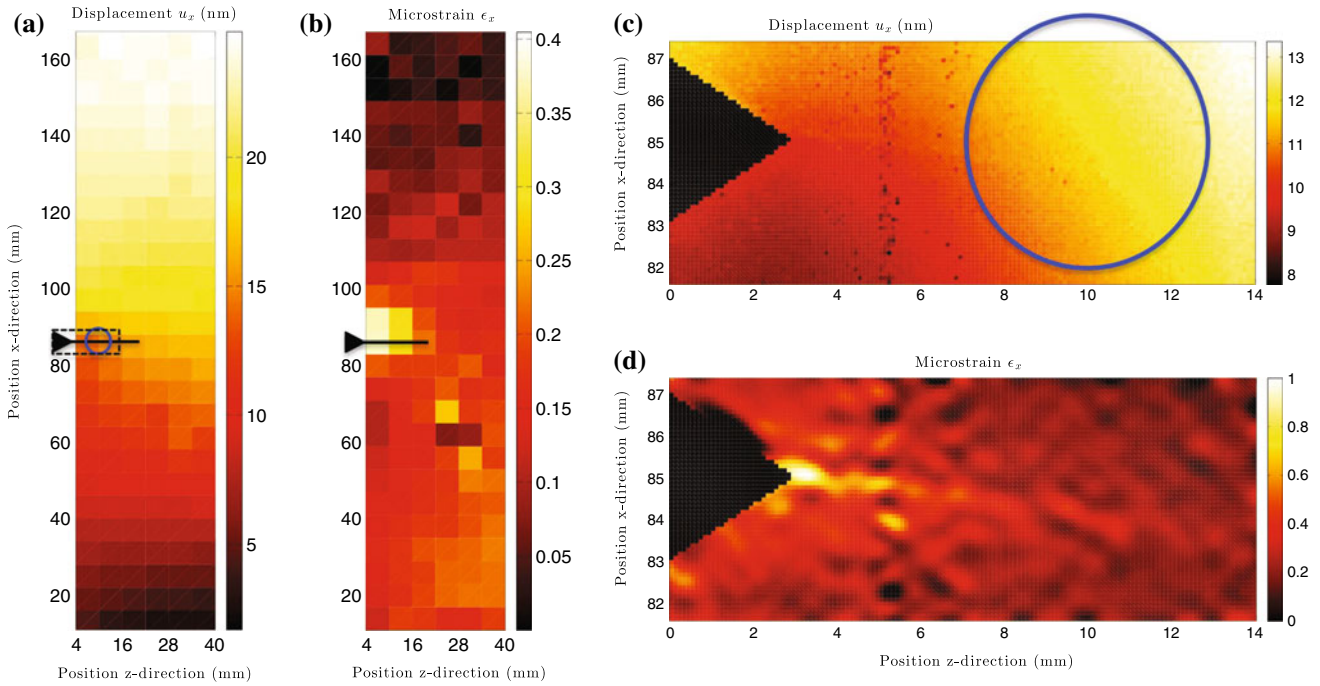

Fig. 4 Field displacement u_x and strain ϵ_x deduced from the experimental scan (setup Fig. 1b). **a**, **b** Field displacement u_x and strain ϵ_x deduced from $\dot{u}_x$. The resolution for this scan is 6mm in both directions. Except for higher strain values noticeable experimentally along the crack, the displacement and strain profiles obtained are the ones expected for a beam with fixed-free boundary conditions. *Black triangles* and *solid lines* represent the position of the notch and the crack. The *dashed rectangle* corresponds to the finer scan presented in (**c**) and (**d**). The *blue solid circle* represents the diameter of the ultrasonic transducer used for ultrasonic linear and DAE measurements when positioned at $[x = h\ ;\ z = 10$ mm]. **c**, **d** Finer scan near the notch region with 0.1 mm-resolution in both directions. Field displacement u_x and strain ϵ_x deduced from $\dot{u}_x$. *Black triangles* represent the position of the notch (Color figure online)

found with this experimental setup will be used in the next section to evaluate the average low frequency strain involved during DAE for each position of the US transducers.

3.3 Nonlinear Results (DAE)

Figure 5 gives an example of DAE results when the US transducers are located at $z = 19$ mm. We observe that when the LF strain is positive (Fig. 5a, tension phase of the sample, crack is open), the ultrasonic velocity is higher than at rest (Fig. 5b), whereas velocity is lower than at rest during the compression phase (negative strain).

A parametric version of Fig. 5 is represented in Fig. 6 for 12 different positions along the width, *i.e.*, relative velocity change as a function of LF strain. We observe some nonlinear signatures all along the crack (Fig. 6a–h), whereas no change

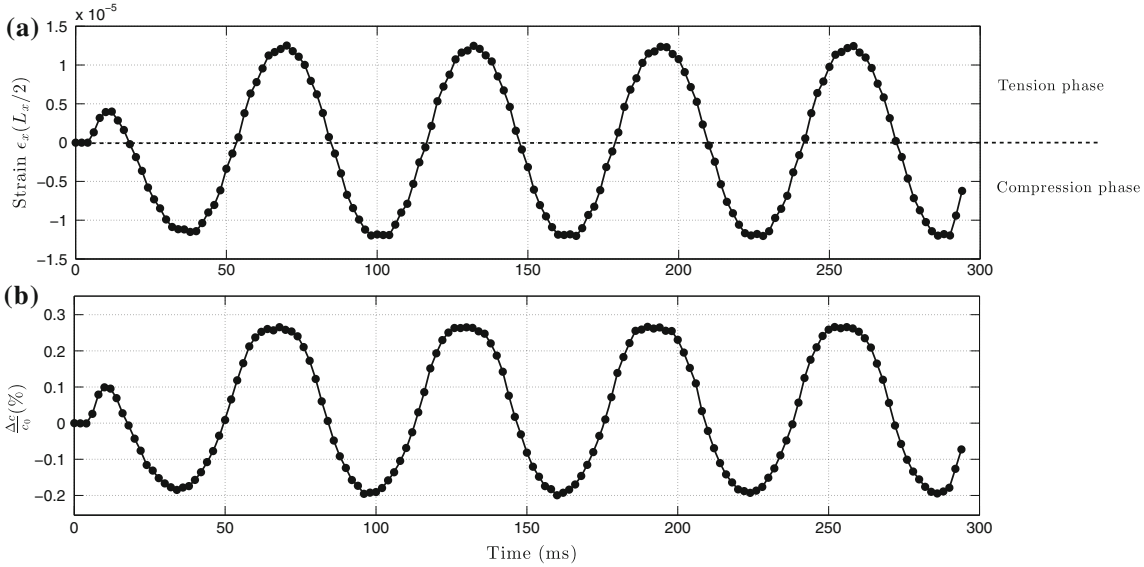

Fig. 5 Example of a DAE result for the position $z = 19$ mm. **a** Strain as a function of time t_j. The time step of 2 ms corresponds to the spacing time ΔT between each ultrasonic pulse broadcast, much larger than the sampling time $t_s = 20$ ns. Therefore, the oscillation period observed here is not T_{LF}, but comes from a combination of both parameters ΔT and T_{LF}, and how incommensurate they are. Positive (respectively negative) strain corresponds to a tension (compression) of the sample. The low frequency source is activated after 5 ms so that the first pulses propagate in the medium without being disturbed by the vibration. Extremum absolute strain is about 1.2×10^{-5}, which corresponds to a 1.4 μm-displacement at 7000 Hz. **b** Relative velocity change as a function of time t_j. Velocity is higher (respectively lower) during the tension (compression) phase

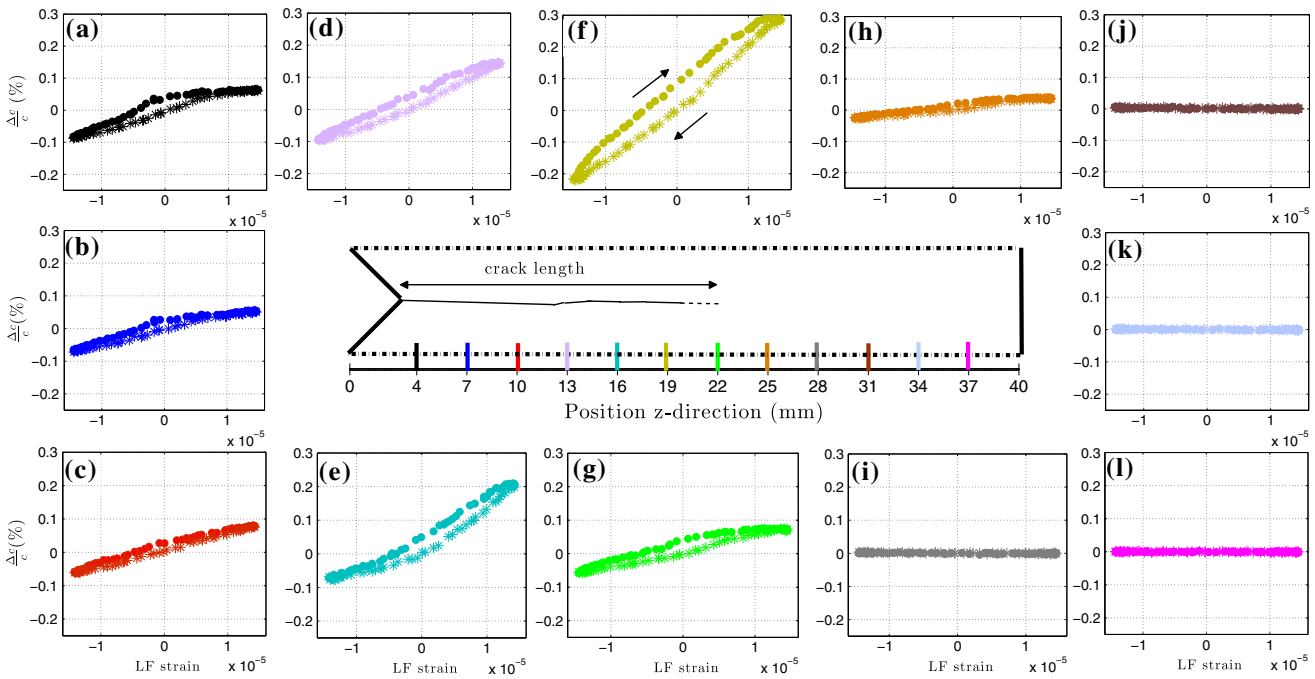

Fig. 6 DAE results for 12 different positions along the sample width L_z. Relative velocity change $\frac{\Delta c}{c}$ is represented as a function of low frequency strain ϵ_x. Positive (negative) strain corresponds to tension (compression) phase of the sample. *Dots* and *stars* correspond to increasing and decreasing strains, respectively. The temporal version of (**f**)-plot is represented in Fig. 5

is observed out of the crack (Fig. 6i–l), meaning that the elasticity away from the crack is essentially linear. Larger slopes and hysteresis are observed near the crack tip (Fig. 6f–g).

Similarly to the result in Fig. 5 ($z = 19$ mm), we observe that the velocity increases during the tension phase, *i.e.* when the crack opens, for all the positions along the crack and near

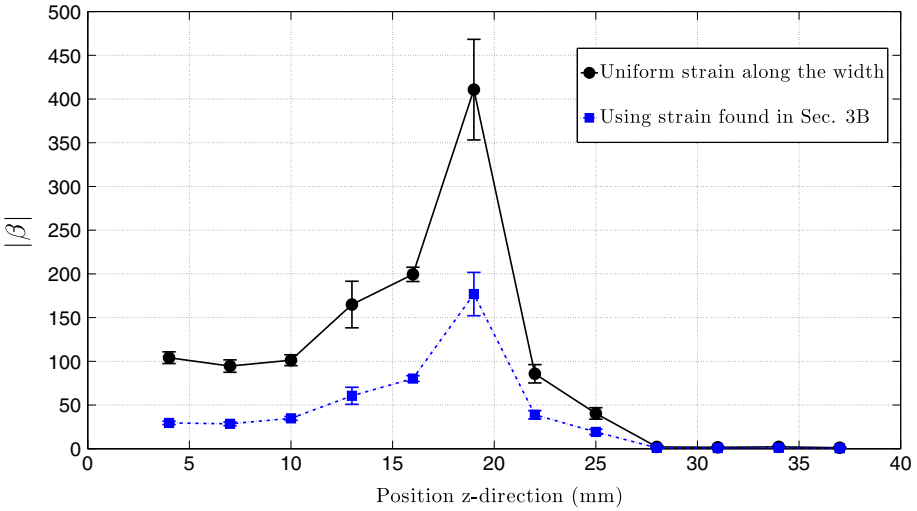

Fig. 7 Nonlinear quadratic elastic parameter β extracted from Fig. 6, using different assumptions to evaluate the strain amplitude of the LF pump. *Solid line* is found assuming that the strain is constant along the sample width (strain not influenced by the crack, $\epsilon_{max} \simeq 1.2 \times 10^{-5}$), see Sect. 2.2.1. The *dashed line* is found by using the actual strain field found in Fig. 4, see Sect. 3.3

the crack tip. Hysteresis is larger near the crack tip (Fig. 6f). Near the notch where the crack is expected to be more open than at any other location, we clearly observe a bi-state behavior (Fig 6a, b), with the presence of a plateau in the tension phase when the crack is opened.

A projection procedure described in detail in [9] is used to extract nonlinear parameters. For the 12 positions, the relative velocity change *versus* time signals $\frac{\Delta c}{c}(t_j)$ in Fig. 5b, taken from 70 to 280 ms during the steady-state regime of the LF resonance, are projected on a series of orthonormal sine and cosine functions ranging from the second harmonic ($n = 1$) to the Nth harmonic ($n = N-1$), *i.e.* $S_n = q_n \sin(2\pi n f_{LF} t_j)$ and $C_n = r_n \cos(2\pi n f_{LF} t_j)$. Amplitudes q_n and r_n are chosen such that these functions are orthonormal [9]. The main interest in using this method is that we can extract the frequency content of a signal that is poorly sampled (the Shannon criteria is not respected since $t_j = 2ms > T_{LF} \simeq 0.14$ms). From this projection, one can extract, for instance, the amount of signal that evolves with ω, $\frac{\Delta c}{c}|_\omega$, which corresponds to the second harmonic content in the signal:

$$\left.\frac{\Delta c}{c}\right|_\omega = \sqrt{\left(\left.\frac{\Delta c}{c}\right|_{\omega_S}\right)^2 + \left(\left.\frac{\Delta c}{c}\right|_{\omega_C}\right)^2} \tag{3}$$

where $\frac{\Delta c}{c}|_{\omega_S}$ (respectively $\frac{\Delta c}{c}|_{\omega_C}$) corresponds to the projection of $\frac{\Delta c}{c}(t_j)$ onto S_1 (respectively C_1), following:

$$\begin{aligned}\left.\frac{\Delta c}{c}\right|_{\omega_S} &= q_1 \sum_{j=1}^{M} S_1(t_j)\frac{\Delta c}{c}(t_j)\\ \left.\frac{\Delta c}{c}\right|_{\omega_C} &= r_1 \sum_{j=1}^{M} C_1(t_j)\frac{\Delta c}{c}(t_j)\end{aligned} \tag{4}$$

with M the total number of points of the experimental signal. The nonlinear quadratic parameter $|\beta|$ is then defined as follows:

$$|\beta| = \frac{2\frac{\Delta c}{c}|_\omega}{\epsilon_{max}} \tag{5}$$

where ϵ_{max} is the maximum strain reached by the LF resonance, approximately 1.2×10^{-5} as seen in Figs. 5 and 6. The parameter β could also be estimated by fitting a 1st-order polynomial on each signature in Fig. 6. Values found with both methods would be equal if no hysteresis is present and if the LF strain field is purely sinusoidal, with no harmonics. Practically, the LF strain field contains harmonics due to the presence of the crack.

In Fig. 7, the solid line represents β calculated as described in Eq. (5), assuming that the maximum strain during the LF resonance is constant along the sample width, $\epsilon_{max} \simeq 1.2 \times 10^{-5}$, as described in Sect. 2.2.1. On the other hand, the dashed line in Fig. 7 corresponds to a correction of the first estimation, taking into account the fact that the strain is not constant along the sample width, as experimentally observed in Fig. 4. A spatially averaged strain value corresponding to the surface of the ultrasonic transducer (blue circle in Fig. 4) at each location along the sample width is extracted from measurements described in Sect. 3.2. In this case, the value ϵ_{max} in Eq. (5) depends on the position of the probed region. Because strain is higher near the notch and along the first centimeters of the crack (Fig. 4), the value β in this region is now lower than initially found with the first assumption. The plot of the nonlinear parameter in this case primarily highlights the crack tip, tightly closed but acting as a very nonlinear spring.

4 Discussion

4.1 Linear Results

Linear velocity measured far from the crack is found to be higher near the boundaries of the sample, when compared to central locations (Fig. 2a). This observation could be due to a hardening effect during the sample cut, slightly increasing the modulus along the surface. The guided nature of the wave propagation along the boundary also implies geometrical dispersion, which could be one other explanation for such difference in velocity. However, we would expect a decrease in (group) velocity along the surface, rather than an increase. Some other simulations could be performed with transducers on the edges of the sample to improve the understanding, however, since our main goal is to focus on nonlinear results and its comparison with linear ones, we consider such analysis as out of scope.

In Fig. 2b, the reason why attenuation is higher experimentally is due to the fact that no dissipation is taken into account in the simulations. We can therefore make a rough estimation of the crack attenuation by taking the difference between the total attenuation (found experimentally) and the attenuation exclusively due to geometrical dispersion (simulation result), that is $8 \pm 4\ m^{-1}$. The mechanisms responsible for the dissipation within the crack remain to be determined.

Further in Fig. 2a, the velocity extracted from simulations remains unchanged whether the crack is present or not, and is slightly lower than found experimentally. The fact that the predicted velocity is smaller than the measured one in Fig. 2 is most likely due to a mismatch between elastic properties used for the simulation and the actual elasticity of the aluminium alloy. Second, the fact that there is no change in velocity in the simulation means that the geometrical dispersion due to the flat crack is not responsible for the measured change in velocity. Several reasons could therefore explain this velocity change along the sample width. The dissipation within the crack (set to zero in the simulation) could contribute to dispersion (dissipative dispersion) and affect the velocity. Furthermore, the simulation assumes a flat crack whereas its more complex geometry could also contribute to a velocity reduction when propagating along the crack.

4.2 DAE (Nonlinear) Results and Comparison with Linear Results

This study represents the first application of DAE to image a single crack in a sample. By probing the sample at different locations along the crack, we highlight different nonlinear elastic features that allow one to better understand how the different parts of the crack respond to the excitation.

Near the notch, the presence of a plateau in the tension phase, *i.e.* no change in velocity when strain changes, means that the crack acts nonlinearly mostly during the compression phase (Fig. 6a, b). It suggests that the crack acts almost linearly in the tension phase. This observation is related to the CAN model (Contact Acoustic Nonlinearity [25,26]) to describe the asymmetry between compression and tension phases. The crack tip is defined by a more symmetric signature and a high nonlinearity (high slopes in Fig 6f, g). It also features a bigger hysteresis, meaning that nonlinear attenuation is mostly taking place at the crack tip. Finally, out of crack in Fig. 6i–l, we find very small nonlinearity ($|\beta| = 1.7 \pm 0.8$) corresponding to the intrinsic (interatomic) nonlinearity of the aluminium sample and in accordance with literature [21]. A quick analysis shows that this value is, however, biased by the Poisson effect occurring during the LF resonance [18]. The Poisson effect and the error found when repositioning the transducers (nearly 50 % of the value) show the limitations of our experimental setup to determine intrinsic nonlinearity of "classic", undamaged materials.

In Fig. 6, the increase in velocity during the tension phase would mean that the direct ultrasonic wave propagating along the crack is less influenced by asperities/friction effects at the crack interface when the latter is opened. On the contrary, velocity decreases during the compression phase, which would imply that asperities at the interface slow down the direct wave. When comparing these results with static acousto-elasticity [27,28], it is somewhat surprising to observe a velocity decrease during the compression phase. Indeed, stiffness at the interface is expected to increase when applying a compressive load. However, stress (strain) involved in static experiments are at least an order of magnitude higher than in DAE, leading to a complete flattening of asperities at the interface and a subsequent increase in the interfacial stiffness. Small stress (strain) involved in DAE might therefore be the reason for such difference. Finally, the fact that the ultrasonic longitudinal pulses propagate normally to the LF oscillation also makes the interpretation difficult since a lateral (tensile) strain in y and z-directions due to the Poisson effect is also present during the compression phase in x-direction. Some DAE measurements are currently ongoing with ultrasonic pulses polarized along the x-direction (main direction of the LF loading/unloading) for comparison.

By comparing linear and nonlinear results (Figs. 2 and 7 respectively), one can observe the higher sensitivity of the nonlinear method which clearly highlights the crack tip in particular. The higher nonlinear response at the crack tip is in agreement with previous time reversal based studies in similar fatigue samples [29,30]. Some other nonlinear parameters could have been presented for comparison, *e.g.* size of the hysteresis or cubic nonlinear parameter extracted from $\frac{\Delta c}{c}|_{2\omega}$. We choose to display only the quadratic nonlinear parameter β and linear parameters, because no other nonlinear parameter is found to be more sensitive than β

for this sample. In Fig. 7, one can notice that the larger the nonlinearity, the larger the error bars (and relative error). Error bars are mostly affected by the repositioning of the US transducers. It therefore means that the region probed by the transducers is slightly changed when repositioning. It suggests that the nonlinearity level near the tip region varies significantly from one location to another. Probing the sample with smaller transducers to increase the spatial resolution could be of great interest to study the crack tip features in more detail.

Another nonlinear parameter of potential interest would be the ratio of second harmonic amplitude to amplitudes of higher harmonics. From Fig. 6, a higher harmonic content is expected at the notch (third harmonic and higher) because of the bi-state behavior between tension and compression phases (Fig. 6a, b), as opposed to the nonlinear signatures observed at the tip (Fig. 6f), where the second harmonic (parameter β) largely dominates over the higher harmonic content. This parameter is not found more sensitive than β for this sample but could be of potential interest for a more open crack for instance, where asymmetric behaviors are more likely to be observed.

Finally, while DAE may not be the easiest nonlinear ultrasonic method to be applied routinely because of geometrical restrictions for the studied sample, it will clearly be of interest to advance the field of nonlinear ultrasonic methods for NDE applications in order to more completely understand the mechanisms of nonlinear elastic behavior of cracks.

5 Conclusion

To the best of our knowledge, this study represents the first application of DAE to a sample with a single crack. By probing the sample at different locations along a closed fatigue crack, we highlight different nonlinear elastic features that allow one to better understand how the different parts of the crack respond to the excitation. More work, including more samples for statistical purposes and more crack types (opened, closed, by fatigue, by corrosion, etc) will have to be done to extend this knowledge and determine which nonlinear parameter is of interest for each crack type and for each crack location (tip side, notch side, etc).

Acknowledgments This research was funded by the U.S. Dept. of Energy, Office of Basic Energy Science (Engineering and Geoscience) and Office of Nuclear Energy (Fuel Cycle R&D, Used Fuel Disposition Campaign).

References

1. Hughes, D.S., Kelly, J.L.: Second-order elastic deformation of solids. Phys. Rev. **92**, 1145–1149 (1953)
2. Winkler, K.W., McGowan, L.: Nonlinear acoustoelastic constants of dry and saturated rocks. J. Geophys. Res. **109**, B10204 (2004)
3. Landau, L.D., Lifshitz, E.M.: Theory of Elasticity, 3rd edn. (Theoretical Physics, vol. 7). Butterworth-Heinemann, (1986)
4. Renaud, G., Rivière, J., Haupert, S., Laugier, P.: Anisotropy of dynamic acoustoelasticity in limestone, influence of conditioning, and comparison with nonlinear resonance spectroscopy. J. Acoust. Soc. Am. **133**, 3706–3718 (2013)
5. Renaud, G., Le Bas, P.Y., Johnson, P.A.: Revealing highly complex elastic nonlinear (anelastic) behavior of earth materials applying a new probe: dynamic acoustoelastic testing. J. Geophys. Res. **117**(B6), B06202 (2012)
6. Renaud, G., Rivière, J., Le Bas, P.Y., Johnson, P.A.: Hysteretic nonlinear elasticity of berea sandstone at low vibrational strain revealed by dynamic acousto-elastic testing. Geophys. Res. Lett. **40**, 715–719 (2013)
7. Guyer, R.A., Johnson, P.A.: Nonlinear Mesoscopic Elasticity: the Complex Behaviour of Rocks, Soil, Concrete. Wiley, New York (2009)
8. TenCate, J.A.: Slow dynamics of earth materials: an experimental overview. Pure Appl. Geophys. **168**(12), 2211–2219 (2011)
9. Rivière, J., Renaud, G., Guyer, R.A., Johnson, P.A.: Pump and probe waves in dynamic acousto-elasticity: comprehensive description and comparison with nonlinear elastic theories. J. Appl. Phys. **114**, 054905 (2013)
10. Ingard, U., Pridmore-Brown, D.C.: Scattering of sound by sound. J. Acoust. Soc. Am. **28**(3), 367–369 (1956)
11. Westervelt, P.J.: Scattering of sound by sound. J. Acoust. Soc. Am. **29**(8), 934–935 (1957)
12. Rollins Jr, F.R., Taylor, L.H., Todd Jr, P.H.: Ultrasonic study of three-phonon interactions. ii. Experimental results. Phys. Rev. **136**(3A), A597 (1964)
13. Taylor, L.H., Rollins Jr, F.R.: Ultrasonic study of three-phonon interactions. i. Theory. Phys. Rev. **136**(3A), A591 (1964)
14. Ohara, Y., Mihara, T., Yamanaka, K.: Effect of adhesion force between crack planes on subharmonic and dc responses in nonlinear ultrasound. Ultrasonics **44**(2), 194–199 (2006)
15. Ohara, Y., Mihara, T., Sasaki, R., Ogata, T., Yamamoto, S., Kishimoto, Y., Yamanaka, K.: Imaging of closed cracks using nonlinear response of elastic waves at subharmonic frequency. Appl. Phys. Lett. **90**(1), 011902–011902 (2007)
16. Ohara, Y., Endo, H., Hashimoto, M., Shintaku, Y., Yamanaka, K.: Monitoring growth of closed fatigue crack using subharmonic phased array. AIP Conf. Proc. **1211**, 903 (2010)
17. Ohara, Y., Endo, H., Mihara, T., Yamanaka, K.: Ultrasonic measurement of closed stress corrosion crack depth using subharmonic phased array. Jpn. J. Appl. Phys. **48**(7), 07GD01-07GD01 (2009)
18. Renaud, G., Talmant, M., Callé, S., Defontaine, M., Laugier, P.: Nonlinear elastodynamics in micro-inhomogeneous solids observed by head-wave based dynamic acoustoelastic testing. J. Acoust. Soc. Am. **130**(6), 3583–3589 (2011)
19. Renaud, G., Callé, S., Defontaine, M.: Remote dynamic acoustoelastic testing: elastic and dissipative acoustic nonlinearities measured under hydrostatic tension and compression. Appl. Phys. Lett. **94**, 011905 (2009)
20. Renaud, G., Callé, S., Defontaine, M.: Dynamic acoustoelastic testing of weakly pre-loaded unconsolidated water-saturated glass beads. J. Acoust. Soc. Am. **128**, 3344 (2010)
21. Hamilton, M.F., Blackstock, D.T.: Nonlinear Acoustics. Academic Press, San Diego (1998)
22. Ulrich, T.J., Van Den Abeele, K., Le Bas, P.Y., Griffa, M., Anderson, B.E., Guyer, R.A.: Three component time reversal: focusing vector components using a scalar source. J. Appl. Phys. **106**(11), 113504–113504 (2009)

23. Sheriff, R.E.: Encyclopedic Dictionary of Exploration Geophysics. Society of Exploration Geophysicists, Tulsa, OK (1991)
24. Tao, H., Zavattieri, P.D., Hector Jr, L.G., Tong, W.: Mode i fracture at spot welds in dual-phase steel: an application of reverse digital image correlation. Exp. Mech. **50**(8), 1199–1212 (2010)
25. Solodov, IYu., Krohn, N., Busse, G.: Can: an example of nonclassical acoustic nonlinearity in solids. Ultrasonics **40**(1), 621–625 (2002)
26. Delrue, S., Van Den Abeele, K.: Three-dimensional finite element simulation of closed delaminations in composite materials. Ultrasonics **52**(2), 315–324 (2012)
27. Biwa, S., Suzuki, A., Ohno, N.: Evaluation of interface wave velocity, reflection coefficients and interfacial stiffnesses of contacting surfaces. Ultrasonics **43**(6), 495–502 (2005)
28. Nagy, P.B.: Ultrasonic classification of imperfect interfaces. J. Nondestr. Eval. **11**(3–4), 127–139 (1992)
29. Ulrich, T.J., Johnson, P.A., Guyer, R.A.: Interaction dynamics of elastic waves with a complex nonlinear scatterer through the use of a time reversal mirror. Phys. Rev. Lett. **98**, 104301 (2007)
30. Ulrich, T.J., Sutin, A.M., Guyer, R.A., Johnson, P.A.: Time reversal and non-linear elastic wave spectroscopy (tr news) techniques. Int. J. Nonlinear Mech. **43**, 209–216 (2008)